K- and *L*-shell ionization of heavy targets by various 20- and 80-MeV/u projectiles

V. L. Kravchuk,[1] A. M. van den Berg,[1] F. Fleurot,[1] M. A. de Huu,[1] H. Löhner,[1] H. W. Wilschut,[1] M. Polasik,[2] M. Lewandowska-Robak,[2] and K. Słabkowska[2]

[1] *Kernfysisch Versneller Instituut, NL-9747AA Groningen, The Netherlands*

[2] *Faculty of Chemistry, Nicholas Copernicus University, Gagarina 7, 87-100 Torún, Poland*

(Received 6 July 2001; published 16 November 2001)

K- and *L*-shell ionization induced by 20 MeV/u He, C, O, and Ne beams on Ta, Pb, and Th targets, and 80 MeV/u He, C, O beams on a Pb target has been studied. *K* x-ray production cross sections have been measured and compared with theoretical calculations. Probabilities of creation of one additional *L*-shell hole, accompanying a *K*-shell hole, have been deduced from experimental data, using the theoretical positions and intensities of the diagram and satellite *K* x-ray lines, obtained from the multiconfiguration Dirac-Fock calculations. This approach avoids explicit measurements of the *L* x-rays and can be applied with the use of a standard Ge detector.

DOI: 10.1103/PhysRevA.64.062710 PACS number(s): 34.50.Fa, 29.30.Kv, 32.30.Rj, 32.70.Jz

I. INTRODUCTION

Until now, the bulk of knowledge concerning inner-shell ionization in ion-atom collisions has been obtained for light projectiles and targets ($Z<50$) [1–7]. The reason for focusing on light systems is the large ionization probability at moderate beam energies, which allows one to measure the relevant observables with relatively simple means. Consequently, not much data are available for heavier systems. One has to rely on extrapolations based on the dominant dependence of the *K*-shell-ionization probability on the reduced velocity $\xi_K \propto v_p/v_K$, i.e., the ratio of the projectile velocity to the *K*-shell-electron velocity, and on the charge of the projectile, Z_p. However, for the heaviest targets $v_K/c \approx 0.6$ and, therefore, relativistic effects become increasingly important [8]. Just as has been done for ^{4}He particles [9,10], explicit measurements for the cases of heavier projectiles and heavy targets are necessary to establish a reliable body of data. Here we study the *K*-shell-ionization cross sections for three targets (Ta, Pb, and Th) and four projectiles (^{4}He, ^{12}C, ^{16}O, and ^{20}Ne) at the same velocity $E/A=20$ MeV/u, and for a Pb target and three projectiles (^{4}He, ^{12}C, ^{16}O) at $E/A=80$ MeV/u, thus we vary both ξ_K and Z_p. The present investigation was made in order to prepare for future nuclear physics experiments in this range of energy and target atomic number.

The observed dependence of the peak positions and the shape of the measured *K* x-ray spectra on the values of Z_p evidences the *L*-shell-ionization accompanying the *K*-shell ionization. Therefore, we have performed a consistent analysis allowing us to establish the *K*-shell-ionization cross sections and the *L*-shell-ionization probabilities simultaneously. The latter measurements have thus been made with a Ge detector and, therefore, avoid the use of low-efficiency crystal spectrometers.

II. EXPERIMENTAL PROCEDURE

The experiment was performed with beams from the superconducting cyclotron AGOR at KVI, Groningen. 20-MeV/u $^4He^{1+}$, $^{12}C^{3+}$, $^{16}O^{4+}$, $^{20}Ne^{5+}$, and 80-MeV/u $^4He^{2+}$, $^{12}C^{6+}$, $^{16}O^{8+}$ ion beams were used. All ions were produced simultaneously in the ECR ion source (ECRIS). The beams were separated by tuning the radio frequency of the cyclotron appropriately [11]. Targets were $^{181}_{73}$Ta, $^{208}_{82}$Pb, and $^{232}_{90}$Th with thicknesses 5.0, 3.6, and 4.8 mg/cm^2, respectively. The uncertainty of the target thicknesses was less than 0.1 mg/cm^2 for each target. Characteristic x-ray spectra were measured with a high-purity Ge-planar x-ray detector with an active area of 100 mm^2, obtained from the Institute for Nuclear Research in Moscow. An energy resolution of $\sigma=255$ eV was obtained at an x-ray energy of 75 keV. Absolute efficiency measurements were made using ^{57}Co, ^{133}Ba, ^{152}Eu, and ^{241}Am standard radioactive sources. The detector was positioned near 90° with respect to the beam direction and outside the scattering chamber at a distance of 30 cm from the target. The chamber window of 1 mm stainless steel effectively removed the intense contribution of *L* x rays on the low-energy side of the spectrum. The typical count rate varied from 1 to 3 kHz, which is sufficiently low to prevent pileup. This was verified by adding a ^{241}Am source during the main runs (except for the runs with the Ta target, where it would interfere with the measurement of Ta *K* x rays). The beam current was integrated in a Faraday cup for normalization. Data were accumulated to have approximately 10^5 counts in the x-ray region to allow for sufficient statistical accuracy in the analysis.

A typical x-ray spectrum is shown in Fig. 1. It has been obtained using a Pb target and a 20-MeV/u ^{4}He beam. The contributions of the various elements and their partition into subcomponents (Siegbahn notation) are indicated. In the analysis for the determination of positions and intensities of the diagram and satellite lines the multiconfiguration Dirac-Fock (MCDF) method has been used (see below).

III. MCDF CALCULATIONS

In recent years, several theoretical models for reliable descriptions of very complex x-ray spectra accompanying the ionization in collision processes based on the MCDF method have been developed and applied [12]. The results of these

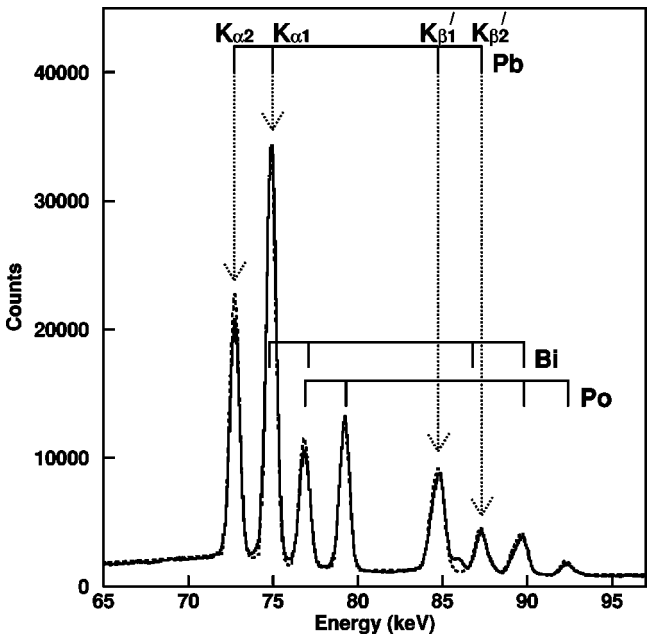

FIG. 1. X-ray spectrum resulting from the reaction 20-MeV/u ^{4}He+^{208}Pb (solid histogram). The dashed line spectrum presents the result of a fitting procedure. Note the γ-ray contribution between the $K\beta$ peaks of Pb.

studies have been successfully implemented in analyses of $K\alpha$ and $K\beta$ x-ray spectra of many target atoms (with $Z>40$) generated in the near-central collisions with various light and heavy projectiles [13–18].

The MCDF method applied in the present study has been described in detail in many papers [19–25]. Therefore, only a brief description will be given here, pointing out the essential details. Within the MCDF scheme the effective Hamiltonian for an N-electron system is expressed by

$$H=\sum_{i=1}^{N} h_D(i)+\sum_{j>i=1}^{N} C_{ij}, \tag{1}$$

where $h_D(i)$ is the Dirac operator for the ith electron and the terms C_{ij} account for electron-electron interactions and come from one-photon exchange process. The latter is a sum of the Coulomb interaction operator (due to longitudinally polarized photons) and the transverse Breit operator (due to transversely polarized photons).

In the MCDF method an atomic-state function with the total angular momentum J and parity π is assumed in the multiconfigurational form

$$\Psi_s(J^\pi)=\sum_m c_m(s)\Phi(\gamma_m J^\pi), \tag{2}$$

where $\Phi(\gamma_m J^\pi)$ are configuration state functions (CSF), $c_m(s)$ are the configuration mixing coefficients for state s, and γ_m represents all information required to uniquely define a certain CSF.

Apart from the transverse (Breit) interaction two types of quantum electrodynamics corrections are included, namely, the self-energy and vacuum-polarization corrections (see McKenzie *et al.* [21]). The formulas for the transition matrix elements and spontaneous emission probabilities can be found in the work of Grant [19]. The calculations have been performed for both the Coulomb and Babushkin [26,27] gauges. In the nonrelativistic limit the Coulomb-gauge formula for the electric dipole transitions yields the dipole velocity expression while the Babushkin formula gives the dipole-length expression [19]. The studies presented in this paper have been done using the GRASP package [25].

IV. DATA ANALYSIS

In the case of collisions of 20-MeV/u ^{4}He with ^{208}Pb the large yields for Bi and Po (which can be seen in the spectrum presented in Fig. 1) indicate the importance of nuclear processes producing the elements of atomic number $Z>Z_T$ (where Z_T refers to the target) and the internal conversion of the decaying residual nuclei [28]. The atomic processes for the produced nuclei ($Z>Z_T$) seem to be insignificant in general, because $\sigma_{nucl}p_K(b=0)\ll\sigma_K$, where $p_K(b=0)$ is the ionization probability and b is the impact parameter that equals zero on the atomic scale. In order to disentangle such spectra, the analysis makes use of a special technique that allows unfolding of the x-ray spectrum into its contributing components. For each measured spectrum we first analyze a single isolated peak (corresponding to a transition energy E_k) in order to obtain a precise description of the response in the detector $P(E-E_k)$. Typically we use five parameters to describe $P(E-E_k)$: a Gaussian of certain width, σ (1 parameter), an exponential tail (3 parameters: a, b, and c, see below) and a Compton tail (1 parameter). Especially important for a good description is the shape of the exponential tail, for which we use $a+b\exp[-(E-E_k)/c]$ in the energy interval from where it connects with the Gaussian at $E=E_k-3\sigma$ down to the backscatter energy $E_k/(1+2E_k/m_ec^2)$.

We assume that the total spectrum is a sum of contributions A_Z^K from the atoms with a single K-shell hole for each element of the atomic number Z (i.e., Z_T for target nuclei and Z_T+1, Z_T+2 for nuclear reaction products) and $A_{Z_T}^{K+L}$ from the target atoms (Z_T) with one K-shell hole and an additional L-shell hole. Therefore, the total spectrum, $X(E)$, can be expressed by

$$X(E)=A_0+\sum_Z A_Z^K\sum_{i=1}^{n}\alpha_i(Z)P(E-E_i(Z)) + A_{Z_T}^{K+L}\sum_{j=1}^{m}\alpha_j(Z_T)P(E-E_j(Z_T)). \tag{3}$$

In this case A_0 is the overall background. The normalized n coefficients α_i describe the relative intensity of the various diagram transitions (with corresponding energies E_i) for the single K-shell hole atomic states of a given element. Similarly, the normalized m coefficients α_j describe the relative intensity of the various satellite transitions (with corresponding energies E_j) for the target atoms with a hole in the K-shell and one additional L-shell hole. The $n=13$ diagram and $m\approx140$ satellite line positions with corresponding rela-

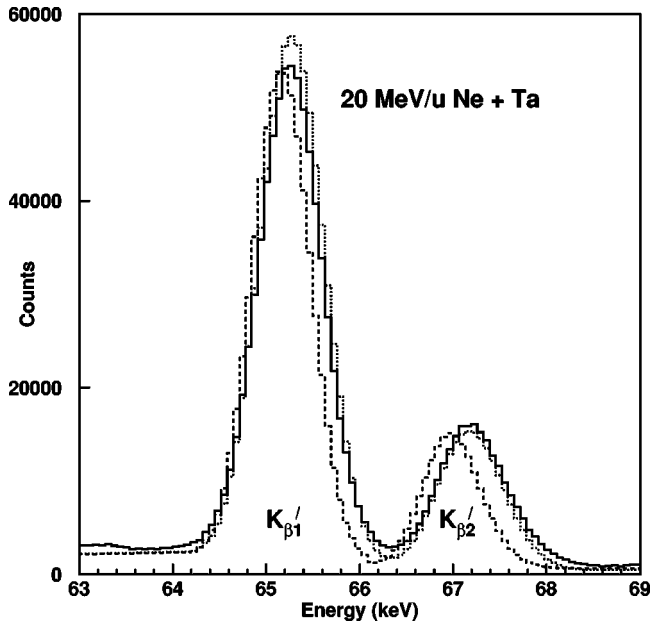

FIG. 2. $K\beta$ region of the x-ray spectrum resulting from the reaction 20-MeV/u ^{20}Ne+^{181}Ta. The solid line presents the experimental data and the dashed line is a fit assuming only single *K*-shell ionization. The dotted line presents a fit assuming *K* plus additional single *L*-shell ionization.

tive intensities have been obtained from the MCDF calculations. By including all possible transitions the same shape can be used for all peaks, in contrast to our earlier work [29] that described the $K\beta$ peaks as a single component instead of a composition of individual transitions.

In order to test the role of the *L*-shell ionization in our experiment, we have initially neglected the contribution from the last term in Eq. (3). The yields A_Z^K and the overall background A_0 have been obtained by a least-square fit that makes use of a simple matrix-inversion technique. This procedure is very effective in excluding from the fit the γ-ray peaks originating from decays following nuclear reactions (as, for example, the γ-ray peak between the K_β peaks of Pb, that can be seen in Fig. 1). In the following we have included these peaks in our analysis by adding one extra peak component to Eq. (3). Although the overall description of the spectra obtained from this simplified procedure is quite satisfactory (see Fig. 1), we observe small discrepancies with the experimental spectra, in particular, for large Z_p and in the $K\beta$ region (see Fig. 2). The excess cross section on the high-energy side of the peaks must be attributed to the additional *L*-shell ionization, as the presence of *L*-shell holes gives the largest shifts in the *K* x-ray energy spectrum. We, therefore, assume that the small shifts due to the M-shell ionization can be ignored, and that at the most a single *L*-shell hole is created. Thus, for a better reproduction of the whole experimental spectra and for evaluation of the *L*-shell-ionization probabilities, now we use Eq. (3), including the last, previously neglected, term. Following the full form of Eq. (3), the characteristic x-ray yields for the target element are assumed to consist of two separate components: one with the total intensity $A_{Z_T}^K$ (for the target atoms with a single *K*-shell hole) and one with the total intensity $A_{Z_T}^{K+L}$ (for the target atoms with a hole in the *K* shell and a hole in the *L* shell).

TABLE I. Experimental *K* x-ray-production cross sections and their errors in barns. The last column gives theoretical KXCROSS code values.

Reaction	E_p(MeV/u)	ξ_K	σ_{KX} $(\Delta\sigma_{KX})$	σ_{KX} (theor)
^{4}He+^{181}Ta	20	0.83	20(2)	16
^{12}C+^{181}Ta	20	0.83	156(15)	124
^{16}O+^{181}Ta	20	0.83	201(19)	210
^{20}Ne+^{181}Ta	20	0.83	290(28)	321
^{4}He+^{208}Pb	20	0.71	9(1)	7
^{12}C+^{208}Pb	20	0.71	65(6)	49
^{16}O+^{208}Pb	20	0.71	78(8)	79
^{20}Ne+^{208}Pb	20	0.71	114(12)	116
^{4}He+^{232}Th	20	0.63	3.3(0.3)	3.1
^{12}C+^{232}Th	20	0.63	25(3)	24
^{16}O+^{232}Th	20	0.63	34(4)	39
^{20}Ne+^{232}Th	20	0.63	43(4)	56
^{4}He+^{208}Pb	80	1.43	44(4)	44
^{12}C+^{208}Pb	80	1.43	389(36)	394
^{16}O+^{208}Pb	80	1.43	704(66)	696

For a description of the shape of the characteristic spectrum of the target atom we thus use positions and relative intensities of approximately 140 diagram and satellite lines, calculated within the MCDF method. A spectrum obtained with the above procedure is shown in Fig. 2 as a dotted line. As can be seen from that figure, the fit assuming *K* plus one additional *L*-shell hole is in much better agreement with the experimental spectrum than the fit that neglects the effect of the additional *L*-shell ionization. Thus, although the individual satellite lines cannot be distinguished, they are crucial for the reproduction of the target-atom spectrum.

For the estimation of the *L*-shell ionization probability per electron, p_L, we have applied the following relation [30]:

$$R_L=\frac{A_{Z_T}^{K+L}}{A_{Z_T}^{K}}=\frac{8p_L}{1-p_L}, \tag{4}$$

where $A_{Z_T}^{K+L}$ and $A_{Z_T}^{K}$ are the total intensities for the target atoms with a hole in the *K* shell and a hole in the *L* shell and for the target atoms with a single *K*-shell hole, respectively. R_L represents also the ratio of the total ionization cross section for production of one *K* hole and one *L* hole to the total ionization cross section for production of one *K* hole and no *L* holes. We can then evaluate the *L*-shell-ionization probability per electron from the expression

$$p_L=\frac{R_L}{8+R_L}. \tag{5}$$

V. RESULTS AND DISCUSSION

A. *K* x-ray cross sections

In Table I the experimental *K* x-ray-production cross sections and their errors are collected. These experimental errors

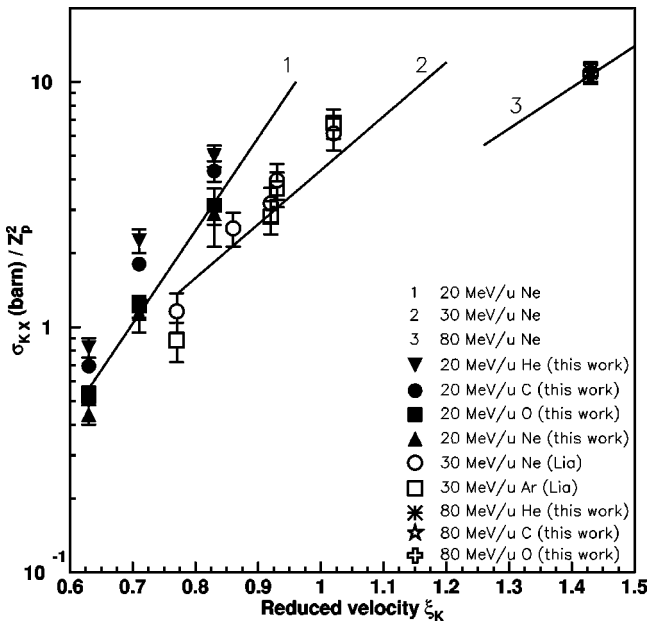

FIG. 3. Experimental reduced *K* x-ray-production cross sections in comparison with KXCROSS code calculations presented as solid lines 1–3 as a function of reduced velocity (ξ_K). Data labeled with Lia have been obtained from [17].

have been deduced using statistical and systematical errors due to uncertainties in the Ge detector efficiency, target thicknesses, and beam current integration. In Fig. 3 the reduced *K* x-ray-production cross sections, i.e., the measured *K* x-ray-production cross sections divided by $Z_p{}^2$, are shown as a function of the reduced velocity ξ_K. In the same figure, the experimental cross sections obtained in the work [31] for 30-MeV/u Ne and Ar projectiles and various targets are also indicated.

To compare the experimental results with the theory we have performed calculations of the direct *K*-shell-ionization cross sections, based on the PWBA-BCPR model, i.e., p(lane) w(ave) b(orn) a(pproximation) method including corrections for b(inding energy effect), c(oulomb deflection), p(olarization effect), and r(elativistic effects) [32–36]. The theoretical values have been computed, using the KXCROSS code based on the formalism described in [29], with the aim to obtain results for different ξ_K. The full results of these calculations are presented in the last column of Table I. In Fig. 3 we show for clarity the theoretical prediction for Ne projectiles only. These are indicated by solid lines labeled 1, 2, and 3, corresponding to 20-, 30-, and 80-MeV/u Ne projectiles, respectively. We observe that the experimental data are systematically higher than the theoretical predictions for the ^{4}He and ^{12}C projectiles, the magnitude is of the order of the experimental error. A similar size systematic deviation but with opposite sign is found for the ^{16}O and ^{20}Ne projectiles result. Therefore, the KXCROSS calculations are quite satisfactory for the description of the experimental cross sections for most of the applications, e.g., for the normalization of nuclear cross sections [29].

B. *L*-shell ionization

The average number of *L*-shell holes, $N_L(=8p_L)$, and the *L*-shell-ionization probabilities per electron, p_L, obtained with the experimental method described in Sec. IV are listed in Table II. There are two sets of data in this table, referring to the two gauges: Coulomb (*C*) and Babushkin (*B*), which have been employed in calculations of diagram and satellite line intensities. The dependence on the gauge is found to be

TABLE II. Average number of *L*-holes, N_L, and *L*-shell-ionization probabilities per electron, p_L, obtained experimentally. $p_L{}^*$ indicates the assumed lower limit for p_L (see text).

Reaction	E_p(MeV/u)	$\overline{\xi_L}$	N_L (*C*)	p_L (*C*)	N_L (*B*)	p_L (*B*)	$p_L{}^*$ (*C*)	$p_L{}^*$ (*B*)
^{4}He+^{181}Ta	20	2.44	0.20	0.025	0.21	0.026	0.023	0.024
^{12}C+^{181}Ta	20	2.44	0.32	0.040	0.35	0.044	0.035	0.038
^{16}O+^{181}Ta	20	2.44	0.46	0.058	0.47	0.059	0.049	0.050
^{20}Ne+^{181}Ta	20	2.44	0.78	0.098	0.79	0.099	0.075	0.076
^{4}He+^{208}Pb	20	2.05	0.11	0.014	0.10	0.013	0.013	0.012
^{12}C+^{208}Pb	20	2.05	0.30	0.037	0.28	0.035	0.033	0.031
^{16}O+^{208}Pb	20	2.05	0.43	0.054	0.41	0.051	0.046	0.044
^{20}Ne+^{208}Pb	20	2.05	0.62	0.078	0.58	0.072	0.063	0.059
^{4}He+^{232}Th	20	1.77	0.37	0.046	0.37	0.047	0.040	0.041
^{12}C+^{232}Th	20	1.77	0.38	0.047	0.37	0.047	0.041	0.041
^{16}O+^{232}Th	20	1.77	0.40	0.050	0.39	0.049	0.043	0.042
^{20}Ne+^{232}Th	20	1.77	0.51	0.064	0.50	0.062	0.053	0.052
^{4}He+^{208}Pb	80	4.10	0.10	0.013	0.10	0.013	0.012	0.012
^{12}C+^{208}Pb	80	4.10	0.11	0.014	0.11	0.014	0.013	0.013
^{16}O+^{208}Pb	80	4.10	0.13	0.016	0.13	0.016	0.015	0.015

less than 10%. We note that the experimental uncertainty due to counting statistics is negligible and the systematical uncertainties noted in Sec. V A do not play an important role here. This is the advantage of using the present approach for calculating *L*-shell ionization probabilities, as they are independent from the experimental conditions. However, in our method we assumed the creation of only one additional *L*-shell hole. Taking into account the binomial distribution of the additional multiple ionization we have estimated the probability of creating a second *L*-shell hole to be less than 10% for ^{4}He, ^{12}C, and ^{16}O projectiles. The maximum probability for a second *L*-shell hole is about 31% in the case of the ^{20}Ne+^{181}Ta reaction. With the assumption that all excess yield $A_{Z_T}^{K+L}$ defined in Sec. IV must be attributed to additional *L*-shell holes, ignoring the details of the corresponding characteristic spectrum,

$$R_L=\frac{A_{Z_T}^{K+L}}{A_{Z_T}^{K}}=\frac{1-(1-p_L)^8}{(1-p_L)^8}, \tag{6}$$

resulting in an alternative value

$$p_L^*=1-\frac{1}{(R_L+1)^{1/8}}. \tag{7}$$

We consider p_L^* to be the lowest limit for p_L. The maximum deviation is 25% also in the ^{20}Ne+^{181}Ta case (see Table II). These conditions also indicate the limits of the method applied in this work. Various other aspects—in particular, the energy calibration and the energy dependence of the detector efficiency—that might affect the deduction of p_L were also investigated. However, requiring a good description of the position of the low-energy side of the x-ray peaks that are not influenced by additional *L*-holes indicated that the result obtained with the present method is robust.

In Fig. 4 the average number of *L*-shell holes, N_L, is shown as a function of Z_p^2. It can be seen from this figure that the *L*-shell-ionization probabilities increase considerably with Z_p^2 in the case of 20-MeV/u projectile energy and Pb and Ta targets, which was also observed in [37] using a Se target. In the case of 80-MeV/u projectile energy and a Pb target the *L*-shell-ionization probabilities are significantly smaller than in the case of 20-MeV/u projectile energy. The reason for this decrease is the large reduced velocity ($\xi_L \propto v_p/v_L$, i.e., the ratio of the projectile velocity to the *L*-shell-electron velocity). In this case ξ_L is about 4, i.e., twice higher than in the 20-MeV/u case and far above the value 1, for which the projectile velocity approximately matches the velocity of the *L*-shell electrons of the target. This dependence is consistent with the recent measurements using light targets (in the $Z=18-39$ region) described in [38]. At higher reduced velocity (80 MeV/u case) we obtained a much less-strong projectile *Z* dependence in the determination of the *L*-shell-ionization probabilities than in the 20 MeV/u case. The reason for this different behavior is presently not understood and will require further investigations both theoretically and experimentally. In particular, for

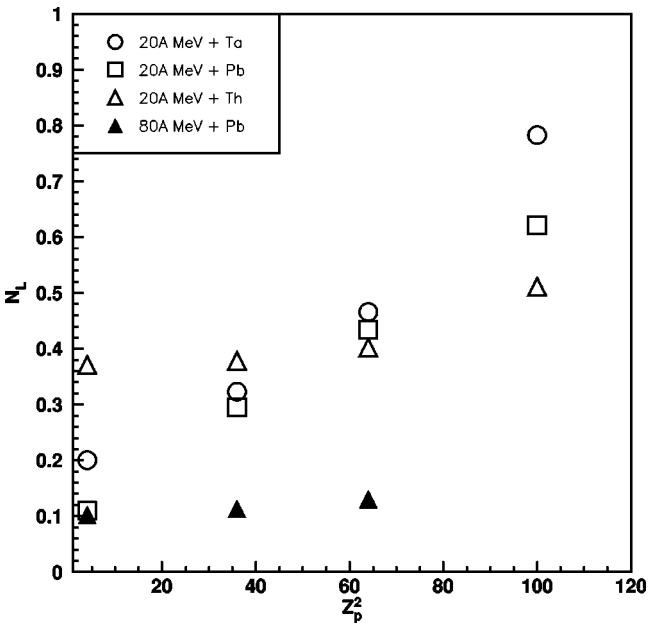

FIG. 4. Average number of *L*-shell holes N_L (based on the Coulomb gauge) as a function of Z_p^2.

α-particle-induced reactions, unforeseen processes following inelastic scattering, involving contributions of internal *L*- and *K*-conversion between nuclear excited states may play a role that is difficult to quantify (cf. the interpretation of the results shown in Fig. 1).

VI. SUMMARY AND CONCLUSIONS

We have studied *K*- and *L*-shell ionization of heavy targets by various projectiles with energies 20 and 80 MeV/u. The *K* x-ray-production cross sections obtained experimentally are within 10% of the theoretical PWBA-BCPR model predictions (KXCROSS code calculations), which shows that this model can be applied in the intermediate reduced velocity regime; the *K* x-ray production cross sections are proportional to Z_p^2.

The approach for the determination of the *L*-shell ionization probabilities using *K* x-ray spectrum, which can be obtained with a standard Ge detector, is presented in this work. The *L*-shell-ionization probabilities have been deduced using the energies and intensities of the diagram and satellite lines obtained from the MCDF calculations. It was found that the experimental values of the *L*-shell-ionization probabilities increase significantly with Z_p^2 in the case of 20-MeV/u projectiles, whereas in the case of 80-MeV/u projectiles and Pb target there is only a slight increase. The effect of *L*-shell ionization is relatively small in studied reactions, in general, less than one *L*-shell hole is created.

The presented results will be used in the interpretation of future experiments concerning the measurement of the fission time scale [39]. In our forthcoming work we will measure the direct ionization cross sections explicitly, which will give us the opportunity to separate the nuclear-process contributions from the *K* x-ray-production cross sections.

ACKNOWLEDGMENTS

We would like to thank the staff of the AGOR Cyclotron and the ECRIS source for providing the various beams during two experiments studied in this paper. This work was performed as part of the research program of the ''Stichting voor Fundamenteel Onderzoek der Materie'' (FOM), which is financially supported by the ''Nederlandse Organisatie voor Wetenschappelijk Onderzoek'' (NWO). This work was partly supported by the Polish Committee for Scientific Research (KBN), Grant No. 2 P03B 019 16.

[1] R. L. Kauffman and P. Richard, Methods Exp. Phys. **13**, 148 (1976).
[2] Proceedings of the Third Workshop on Inner Shell Ionization by Light Ions, Nucl. Instrum. Methods Phys. Res. B **232** (1984).
[3] B. Perny, J.-Cl. Dousse, M. Gasser, J. Kern, Ch. Rhême, P. Rymuza, and Z. Sujkowski, Phys. Rev. A **36**, 2120 (1987).
[4] P. Rymuza, Z. Sujkowski, M. Carlen, J.-Cl. Dousse, M. Gasser, J. Kern, B. Perny, and Ch. Rhême, Z. Phys. D: At., Mol. Clusters **14**, 37 (1989).
[5] P. Rymuza, T. Ludziejewski, Z. Sujkowski, M. Carlen, J.-Cl. Dousse, M. Gasser, J. Kern, and Ch. Rhême, Z. Phys. D: At., Mol. Clusters **23**, 81 (1992).
[6] I. Orlic, Nucl. Instrum. Methods Phys. Res. B **87**, 285 (1994).
[7] M. Kavcic, M. Budnar, A. Muhleisen, P. Pelicon, Z. Smit, M. Zitnik, D. Castella, D. Corminboeuf, J.-C. Dousse, J. Hoszowska, P. A. Raboud, and K. Tokesi, Phys. Rev. A **61**, 052711 (2000).
[8] D. Mitra, Y. Singh, L. C. Tribedi, P. N. Tandon, and D. Trautmann, Phys. Rev. A **64**, 012718 (2001).
[9] M. Dost, S. Hoppenau, S. Röhl, and W. A. Schönfeldt, J. Phys. B **14**, 3153 (1981).
[10] H. Paul and O. Bolik, At. Data Nucl. Data Tables **54**, 75 (1993).
[11] H. W. Schreuder, in *Proceedings of the Fifteenth International Conference on Cyclotrons and their Applications, Caen, France, 1998*, edited by E. Baron and M. Lieuvin (Institute of Physics, Bristol), p. 592.
[12] M. Polasik, Phys. Rev. A **39**, 616 (1989); **39**, 5092 (1989); **40**, 4361 (1989); **41**, 3689 (1990); **52**, 227 (1995).
[13] M. W. Carlen, M. Polasik, B. Boschung, J.-Cl. Dousse, M. Gasser, Z. Halabuka, J. Hoszowska, J. Kern, B. Perny, Ch. Rhême, P. Rymuza, and Z. Sujkowski, Phys. Rev. A **46**, 3893 (1992).
[14] M. W. Carlen, B. Boschung, J.-Cl. Dousse, M. Gasser, Z. Halabuka, J. Hoszowska, J. Kern, B. Perny, Ch. Rhême, M. Polasik, P. Rymuza, and Z. Sujkowski, Phys. Rev. A **49**, 2524 (1994).
[15] T. Ludziejewski, P. Rymuza, Z. Sujkowski, B. Boschung, J.-Cl. Dousse, B. Galley, Z. Halabuka, Ch. Herren, J. Hoszowska, J. Kern, Ch. Rhême, and M. Polasik, Phys. Rev. A **52**, 2791 (1995).
[16] T. Ludziejewski, P. Rymuza, Z. Sujkowski, G. Borchert, J.-Cl. Dousse, Ch. Rhême, and M. Polasik, Phys. Rev. A **54**, 232 (1996).
[17] Ch. Herren, B. Boschung, J.-Cl. Dousse, B. Galley, J. Hoszowska, Ch. Rhême, M. Polasik, T. Ludziejewski, P. Rymuza, and Z. Sujkowski, Phys. Rev. A **57**, 235 (1998).
[18] B. Galley, B. Boschung, J.-Cl. Dousse, Ch. Herren, J. Hoszowska, J. Kern, Ch. Rhême, M. Polasik, T. Ludziejewski, P. Rymuza, and Z. Sujkowski, Phys. Rev. A (to be published).
[19] I. P. Grant, J. Phys. B **7**, 1458 (1974).
[20] I. P. Grant, B. J. McKenzie, P. H. Norrington, D. F. Mayers, and N. C. Pyper, Comput. Phys. Commun. **21**, 207 (1980).
[21] B. J. McKenzie, I. P. Grant, and P. H. Norrington, Comput. Phys. Commun. **21**, 233 (1980).
[22] I. P. Grant and B. J. McKenzie, J. Phys. B **13**, 2671 (1980).
[23] J. Hata and I. P. Grant, J. Phys. B **16**, 3713 (1983).
[24] I. P. Grant, Int. J. Quantum Chem. **25**, 23 (1984).
[25] K. G. Dyall, I. P. Grant, C. T. Johnson, F. A. Parpia, and E. P. Plummer, Comput. Phys. Commun. **55**, 425 (1989).
[26] F. A. Babushkin, Opt. Spectrosc. **13**, 77 (1962).
[27] F. A. Babushkin, Acta Phys. Pol. **25**, 749 (1964).
[28] G. J. Balster, H. W. Wilschut, R. H. Siemssen, P. C. N. Crouzen, P. B. Goldhoorn, and Z. Sujkowski, Nucl. Phys. A **468**, 131 (1987).
[29] G. J. Balster, W. van Huffelen, H. W. Wilschut, D. Chmielewska, and Z. Sujkowski, Z. Phys. D: At., Mol. Clusters **2**, 15 (1986).
[30] B. Boschung, M. W. Carlen, J.-Cl. Dousse, B. Galley, Ch. Herren, J. Hoszowska, J. Kern, Ch. Rhême, T. Ludziejewski, P. Rymuza, Z. Sujkowski, and Z. Halabuka, Phys. Rev. A **52**, 3889 (1995).
[31] E. Liatard, J. F. Bruandet, F. Glasser, Tsan Ung Chan, G. J. Costa, C. Gérardin, C. Heitz, M. Samri, and R. Seltz, Z. Phys. D: At., Mol. Clusters **2**, 223 (1986).
[32] G. Basbas, W. Brandt, and R. Laubert, Phys. Rev. A **7**, 983 (1973).
[33] G. Basbas, W. Brandt, and R. Laubert, Phys. Rev. A **17**, 1655 (1978).
[34] R. Anholt, Phys. Rev. A **17**, 983 (1978).
[35] P. A. Amundsen, L. Kocbach, and J. M. Hansteen, J. Phys. B **9**, L203 (1976).
[36] R. Rice, G. Basbas, and F. D. McDaniel, At. Data Nucl. Data Tables **20**, 503 (1977).
[37] M. Polasik, S. Raj, B. B. Dhal, H. Padhi, A. K. Saha, M. B. Kurup, K. G. Prasad, and P. N. Tandon, J. Phys. B **32**, 3711 (1999).
[38] Y. Awaya, T. Kambara, and Y. Kanai, Int. J. Mass Spectrom. **192**, 49 (1999).
[39] Proposal R18, KVI, Groningen, 2000.